Bull Volcanol (2016) 78: 74
DOI 10.1007/s00445-016-1070-z

RESEARCH ARTICLE

Shallow conduit processes during the AD 1158 explosive eruption of Hekla volcano, Iceland

Maria H. Janebo[1,2] · **Bruce F. Houghton**[1] · **Thorvaldur Thordarson**[3] · **Gudrun Larsen**[4]

Received: 18 February 2016 / Accepted: 11 September 2016 / Published online: 1 October 2016

Abstract Hekla is one of the most frequently active felsic volcanic systems in the world, with several known pre-historic large Plinian eruptions and 18 historical subplinian to small Plinian eruptions. A common view is that Plinian eruptions of Hekla are relatively short lived and purely explosive events. In detail, these events exhibit subtle differences in terms of deposit characteristics, reflecting significant differences in eruption behaviour. Of the 18 historical eruptions, two had bulk magma compositions with >66 wt% SiO_2: a Plinian eruption in AD 1104 and a smaller, less well characterised, but atypical subplinian eruption in AD 1158. The AD 1158 eruption was a relatively sustained, dry (magmatic) eruption with a more powerful opening phase followed by a lower intensity, waning phase accompanied by minor destabilisation and collapse of the conduit walls. We examine here the dynamics of the AD 1158 eruption, focussing on the role of shallow conduit processes in modulating eruption dynamics. Vesicularity data constrain the relative influence of bubble nucleation, growth, and coalescence. The juvenile pyroclasts are composed of two types of microvesicular pumice (white and grey) with contrasting vesicle number density, vesicle-size distribution, and phenocryst and microlite contents. Textural analysis shows that these pumices reflect heterogeneity developed pre- to syn-eruptively in the conduit and that entrainment of longer resident magma by faster ascending magma permitted magma of contrasting maturity to be fragmented simultaneously. In this regard, the mixed melt of the AD 1158 eruption contrasts with the compositionally homogeneous melt phase of the more powerful AD 1104 Plinian event, which was typified by more uniform conduit and eruption dynamics accompanying higher average ascent rates.

Keywords Hekla volcano · Plinian eruptions · Eruption style · Vesicle number density

Editorial responsibility: J.E. Gardner

Electronic supplementary material The online version of this article (doi:10.1007/s00445-016-1070-z) contains supplementary material, which is available to authorized users.

✉ Maria H. Janebo
janebo@hawaii.edu

[1] Department of Geology and Geophysics, SOEST, University of Hawai'i at Mānoa, Honolulu, HI 96822, USA

[2] Present address: Nordic Volcanological Center, Institute of Earth Sciences, University of Iceland, Reykjavik, Iceland

[3] Faculty of Earth Sciences, University of Iceland, Reykjavik, Iceland

[4] Institute of Earth Sciences, University of Iceland, Reykjavik, Iceland

Introduction

Hekla, located at the southwest flank of the East Volcanic Zone (Fig. 1a), is one of the most active volcanic systems in Iceland. It has featured a series of pre-historic large Plinian eruptions (e.g. Larsen and Thorarinsson 1977; Larsen and Eiríksson 2008b; Gudmundsdóttir et al. 2011), notably the H3, H4, and H5 eruptions at about 3000 BP, 4200 BP, and 7000 BP, respectively (Larsen and Eiríksson 2008a; Thordarson and Höskuldsson 2008), and 18 historical subplinian to smaller Plinian eruptions (Thordarson and Larsen 2007). Due to the frequent historical activity, the explosive behaviour of Hekla is well characterised. In general, the eruption volume and the silica content of the erupted melt increases with increasing repose time (Thorarinsson 1967). Explosive activity at the central volcano may be of two types: (1) a short, intense purely Plinian eruption lasting hours, or (2)

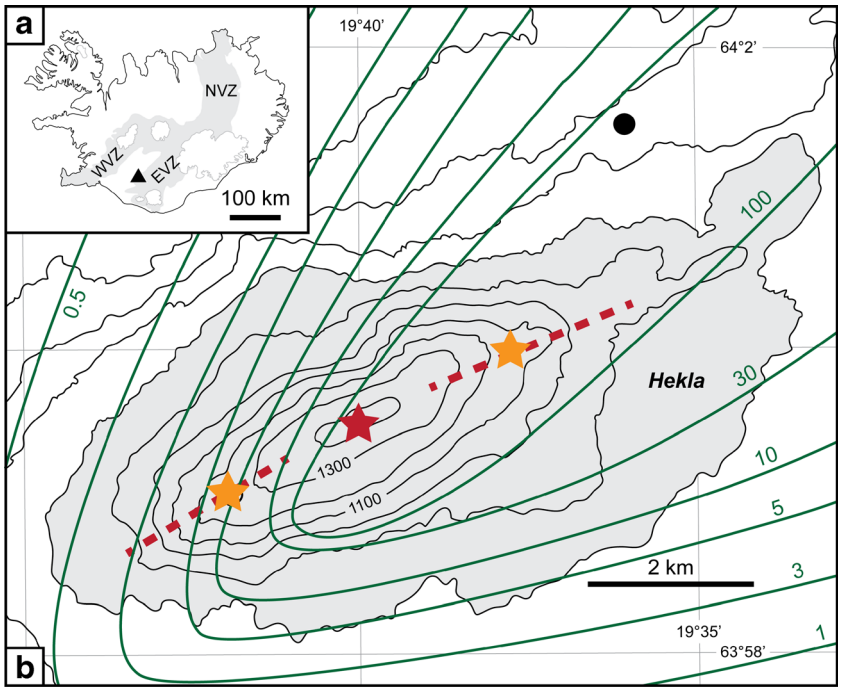

Fig. 1 **a** Map of Iceland with the three main active volcanic regions shown in grey (*NVZ* North Volcanic Zone, *WVZ* West Volcanic Zone, *EVZ* East Volcanic Zone). Location of Hekla indicated by the *black triangle*. **b** Map of Hekla with location of the type section for the 1158 eruption (*black dot*: 64° 1.466′ N, 19° 36.080′ W). *Red dashed line* shows the position of the Hekla fissure, *red star* the summit vent and *orange stars* the shoulder vents. Topographic contour interval 100 m. *Isopach lines* (Janebo et al. 2016) in *green* with thickness values in cm

a hybrid eruption starting with a Plinian or subplinian phase followed by prolonged Strombolian activity and lava flows (Thordarson and Larsen 2007). Type 1 activity may be confined to the summit area, whereas type 2 activity typically starts there and then expands to the larger vent system (Fig. 1b). All the well-constrained historical Plinian and subplinian phases were short, typically less than a few hours, and typified by high eruption rate in the range from ~1000 to ~25,000 m^3 s^{-1} (Gronvold et al. 1983; Höskuldsson et al. 2007; Thordarson and Larsen 2007).

Only two historical eruptions have had bulk magma compositions with >66 wt% SiO_2: the Plinian eruption in AD 1104 (also known as the H1 event) and the smaller, and to date, less well-characterised eruption in AD 1158. The initial magma compositions were rhyolitic (70–73 wt% SiO_2), and dacitic (65–68 wt% SiO_2), respectively (Larsen et al. 1999).

The eruption of 19 January 1158 (Thorarinsson 1967) deposited an estimated 0.33 km^3 (unconsolidated, 0.2 km^3 consolidated) tephra over parts of eastern Iceland (Larsen 1992, 2002). There are no constraints on the duration, but the eruption likely lasted less than a few hours to maximum a day. Based on the isopach map (Larsen 1992), there is no indication of a change in wind direction during the eruption. The AD 1158 eruption is atypical for Hekla. It both contrasts with and is similar to the older purely Plinian eruptions and the younger subplinian opening phases. The eruption was subplinian in dispersal, and the 0.1 km^3 lava flow Háahraun, which has the same composition as the AD 1158 tephra, is believed to be associated with the AD 1158 eruption (Sigmarsson et al. 1992). The magma composition is relatively evolved for the quite short 54-year repose time since AD 1104, and the juvenile ejecta contain white, grey, and banded pumices of contrasting vesicularity and crystallinity (Fig. 2).

The presence of white and grey (and banded) pumices has been observed in numerous eruptions at Hekla and elsewhere. Such a difference between the two pumice types at other volcanoes is either compositional (Lirer et al. 1973) or textural caused by differences in the microlite content and vesicularity (Klug and Cashman 1994; Polacci et al. 2001), or a combination of both (Wright et al. 2011).

Several of the pre-historic Hekla eruptions have two distinct pumice populations of contrasting composition, namely, white rhyolitic pumice and dark grey andesitic pumice. In the deposits, a white pumice layer is overlain by a greyish brown pumice layer. Especially in the zoned Hekla H-A to H-Z eruptions (Larsen and Vilmundardóttir 1992; Róbertsdóttir et al. 2002), the shift from yellow-white or greyish-yellow to dark

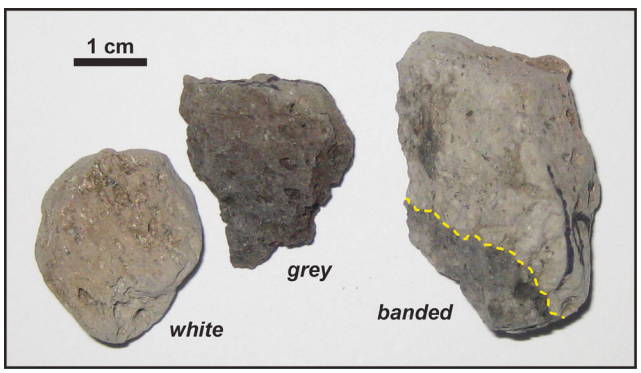

Fig. 2 Photo of pumice types from the Hekla 1158 eruption: white, grey, and banded clasts. *Dashed yellow line* marks the contact between a grey band in a white pumice clast

grey pumice is abrupt, without any significant break in grain size and sorting (thereby indicating that these are from a fairly continuous steady eruption). For the AD 1158 eruption, which was much smaller in volume and lower in intensity than most of these zoned eruptions, there is no significant compositional difference between the white and grey pumices (see supplementary Table 1) and both were erupted, in varying proportions throughout the entire eruption. We suggest below that the white (glassy) and grey (microlite-rich) pumices are more likely derived from a single, initially chemically and texturally homogeneous melt by contrasting patterns of ascent and degassing/outgassing in the shallow conduit, rather than resulting from the tapping and orderly evacuation of a chemically zoned magma body.

Methodology

A type section was defined about 5 km downwind from the summit vent (Fig. 1b), where the AD 1158 deposit is the thickest, a little over 1.5 m thick. To investigate changes over time, the deposit was divided into eight equal intervals (Fig. 3a) that were sampled for grain size and four larger equal intervals (Fig. 4a) that were sampled for clast density/vesicularity analysis. Grain size analysis was conducted, using standard sieving techniques, down to 4 ϕ (63 μm, with $\phi = -\log_2(d)$ and d being the particle diameter in mm). Median diameter (Md_ϕ) and sorting coefficients (σ_ϕ) were calculated following Inman (1952). Componentry analysis was done on all clasts >2 mm in diameter, corresponding to a minimum of 85 wt% of each grain size sample.

The density of 100 juvenile clasts, with diameters of 16 to 32 mm, from each sample interval was determined following Houghton and Wilson (1989). A dense rock equivalent (DRE) value of 2350 kg m^{-3} was used when converting from measured density to calculated vesicularity. Quantitative vesicularity analysis was performed on nine juvenile clasts, representative of the range of pumice types: one pair of modal density white and grey pumices from each stratigraphic level and one additional highly vesicular white pumice, following Shea et al. (2010). Nested image sets were constructed from 1200 dpi scans of the thin sections combined with back-scattered electron (BSE) images at four magnifications (25×, 100×, 250× and 500×) collected using a JEOL-5900LV scanning electron microscope (SEM) operating at 15 kV accelerating voltage and 1 nA beam current. All images were converted to binary format and rectified in Adobe Photoshop, and quantitative vesicle analysis was performed using the ImageJ software (Schneider et al. 2012). The 2-D areal vesicle number density (N_A) was adjusted for the presence of phenocrysts and converted to 3-D volumetric vesicle number density (N_V) using the method of Sahagian and Proussevitch (1998). N_V is referenced to melt volume (N_{Vm}) in order to account for the presence of the vesicles (Klug et al. 2002). In total, 23 images were analysed for each clast. The lower size limit of analysed vesicles included in the vesicle-size distribution was set to 4 μm, equivalent to a cut-off value of 20 and 10 pixels in the 500 (white pumice) and 250 (grey pumice) magnification images, respectively. The effect of the choice of lower size limit of analysed vesicles on the resulting vesicle number density (VND) is discussed in supplementary document 1.

Results

Deposit characteristics

At the type section, the deposit consists of two parts: a lower, coarser part and an upper, slightly finer part (Fig. 3). The juvenile material comprises two types of microvesicular pumice (white and grey in colour), which are present both as discrete clasts and as mingled or banded clasts (Fig. 2). The white pumice is dominant in all samples, and the mingled clasts are generally white with mm to cm-thick grey bands. The lithic component consists of grey and red lava clasts, probably derived from the conduit walls.

All grain size samples are unimodal, with a median diameter in the range of −4.4 to −4.1 ϕ (22 to 17 mm) in the lower half of the deposit, fining to −3.7 to −2.4 ϕ (13 to 5 mm) in the upper part. The deposit is very well to well sorted (σ_ϕ 0.83 to 1.4) throughout (Fig. 3b).

The abundance of white pumice increases upwards slightly in the lower section and then decreases in the upper section, whereas the grey and banded pumices show the opposite trend (Fig. 3d). White pumice ranges from 81 to 93 wt% of the juvenile fractions. Wall-rock lithic clasts range in abundance from 3 to 8 wt%. The lithic abundance is high in the lowermost sample, decreases slightly towards the middle of the deposit and then increases towards the top of the deposit (Fig. 3c).

Clast density

All density samples show similar positively skewed unimodal distributions with a denser tail (Fig. 5). The main peak is dominantly white pumice, the denser tail grey pumice, and the banded pumice predictably spans the range of the two endmembers. The mean density ranges from 480 to 600 kg m^{-3} for the total samples and 450 to 540 kg m^{-3} for the white pumice only

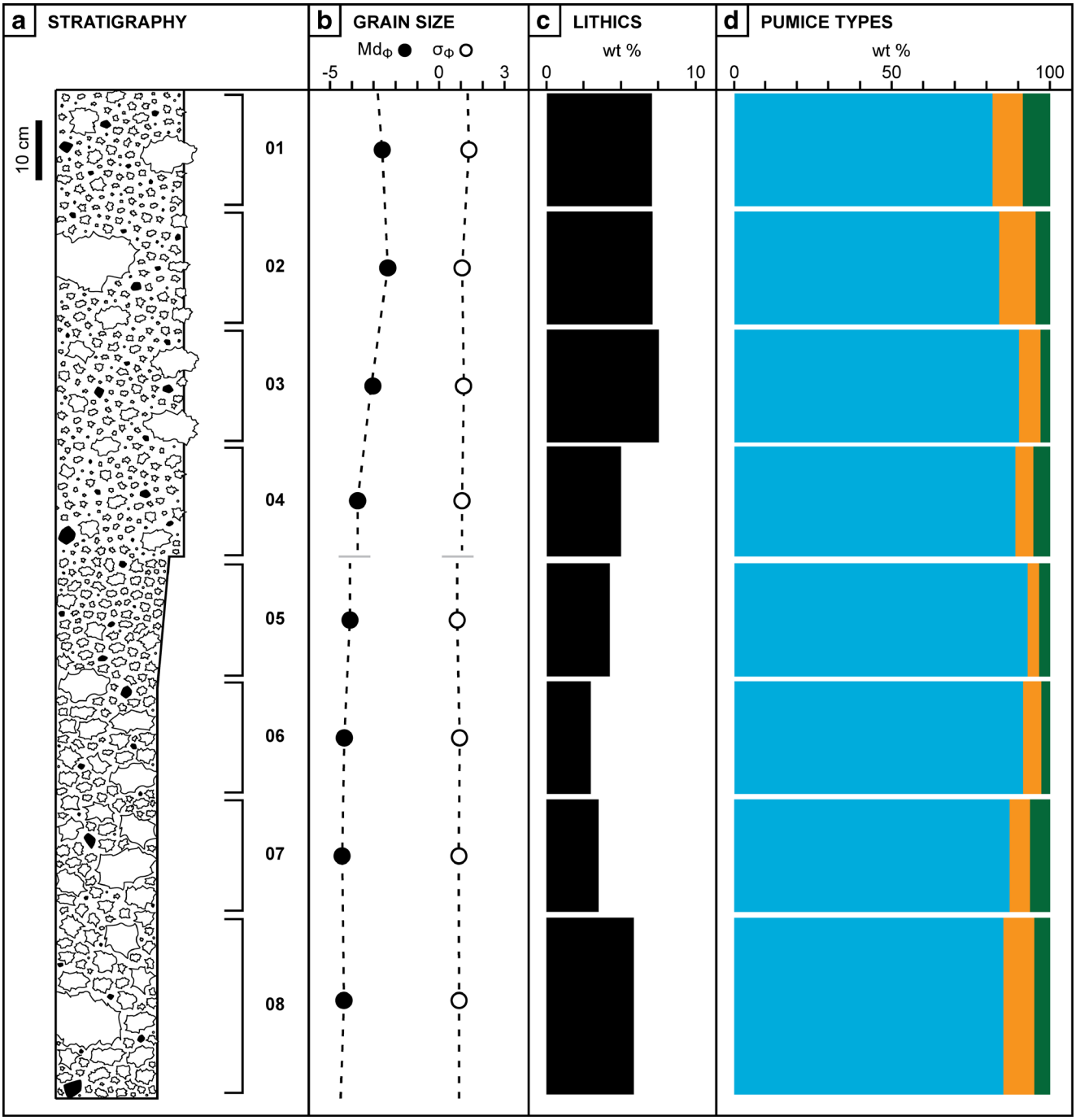

Fig. 3 **a** Stratigraphic log of the Hekla 1158 deposit with intervals sampled for grain size and componentry analysis. Samples are numbered from the *top* to the *bottom* of the deposit. **b** Results from grain size analysis. Median diameter is showed in *filled circles* and sorting in *open circles*. **c** Lithic abundance. **d** Proportion of pumice types (normalised to 100 %) with white pumice in *blue*, grey pumice in *orange*, and banded pumice in *green*

(Fig. 4), corresponding to a mean calculated vesicularity of 74 to 80 vol.% (total) or 77 to 81 vol.% (white pumice only). There is no clear temporal trend in the density data, but the widest distribution within the white pumice (with a range of 310 to 900 kg m^{-3}, 62 to 87 vol.% vesicularity) occurs in the upper middle part of the deposit. The mode of the density distribution also alternates between 400–500 and 500–600 kg m^{-3} with successive samples (Fig. 5).

Quantitative vesicularity and textural analysis

The nine clasts chosen for detailed textural analysis are all internally heterogeneous, containing populations of large

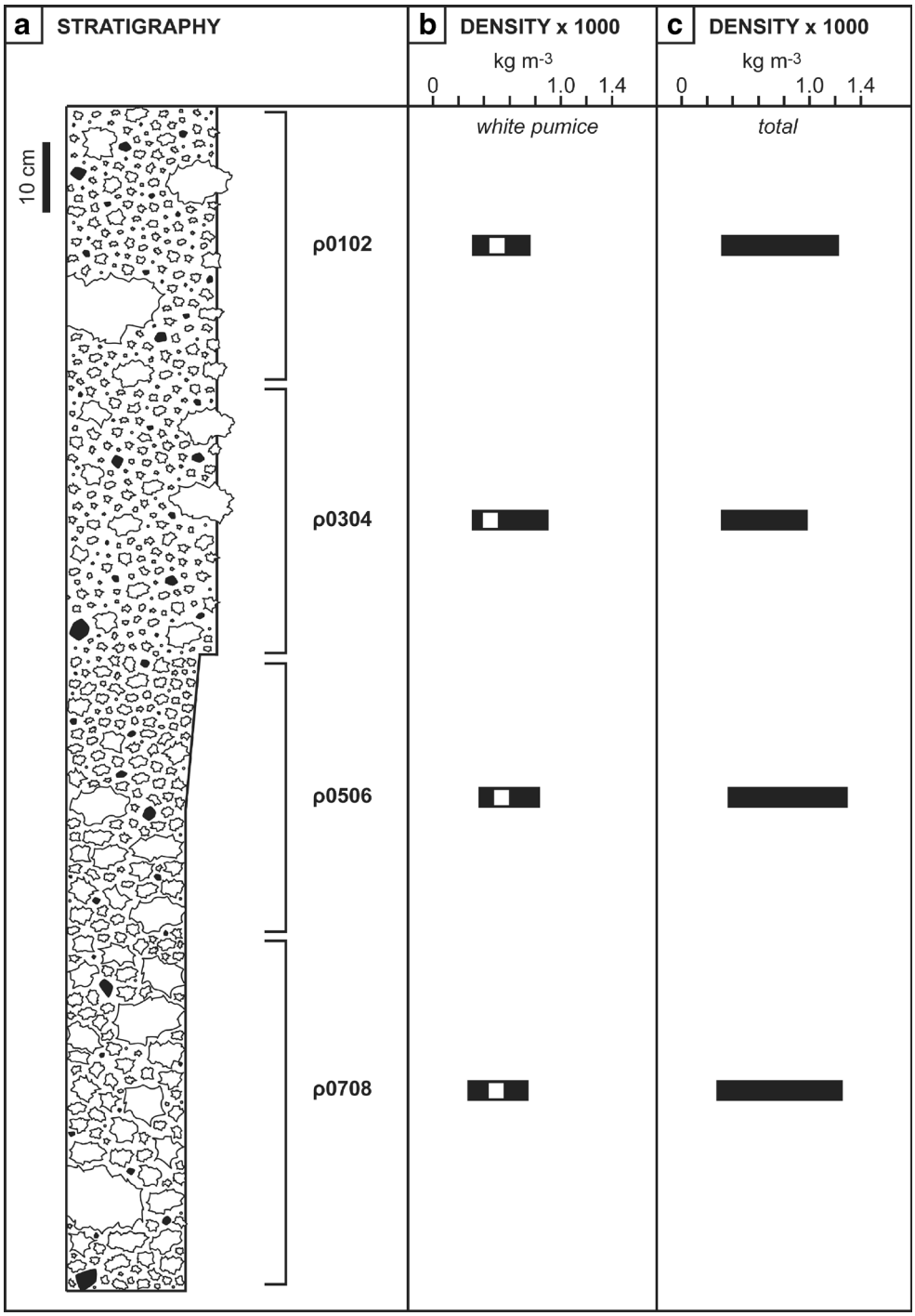

Fig. 4 **a** Stratigraphic log of the Hekla 1158 deposit with intervals sampled for vesicularity analysis. Samples are numbered from the *top* to the *bottom* of the deposit. **b** Mean density of the white pumice is shown by *open square*, and range in density of white pumice is shown by the *thick bar*. **c** Range in density of all pumice

(>150 μm to mm sized) vesicles surrounded by intermediate to small (150 to <25 μm) vesicles (Fig. 6). In thin section, vesicle shapes range from round or elongate to convoluted polylobate. Evidences of coalescence (Fig. 7), such as wall rupture, thin planar melt films, and small vesicles enclosed inside larger vesicles (described as donuts or 'donut-like' features in previous studies; Klug et al. 2002; Adams et al. 2006), are present in all clasts. The crystal content was not quantified, but all clasts contain both phenocrysts and microlites.

The vesicle volume distributions (VVDs) are mostly unimodal with tails of vesicles up to about 3 mm in diameter superimposed on broad modes of approximately 125–200 μm (Fig. 8). The VVDs for the four modal white pumice clasts are very similar. VVDs for the grey clasts are less homogeneous, and the clasts from the

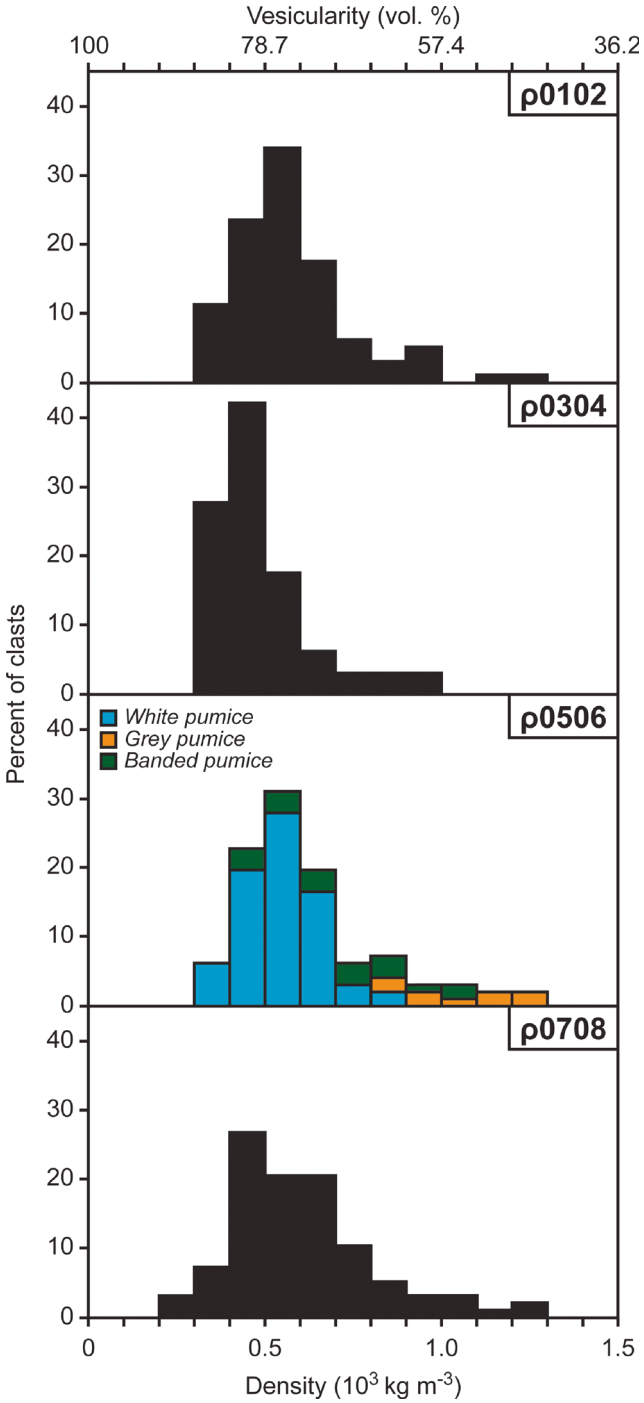

Fig. 5 Pumice density histograms for the Hekla 1158 deposit, with clast types overlain for sample ρ0506

stratigraphically lowest (ρ0708) and highest (ρ0102) samples are weakly bimodal. All clasts have sigmoidal cumulative vesicle volume distributions (CVVDs) (Fig. 9), and the median vesicle diameter is between 40 and 100 μm (Table 1).

The cumulative vesicle-size distributions (CVSDs) for all clasts are shown in Fig. 10 as log plots of melt-corrected number density (N_{Vm}) of vesicles greater than diameter L. In every sample, the moderate to large vesicle population can be best fit by a power law with an exponent of −3.5 to −4. The much larger number of the smaller vesicles (<25 and <40 μm in the white and grey pumice, respectively), however, is better described by an exponential fit.

The melt-corrected vesicle number densities (N_{Vm}) range from 1.51×10^8 to 1.04×10^9 cm^{-3} (Table 1). Decreasing the lower size limit of analysed vesicles included in the vesicle size distribution to 2 μm increases the measured N_A by a factor of 1.03 to 1.09 but does not significantly change the derivative N_{Vm} values (average increase <10 %; supplementary document 1). Although all are within one order of magnitude, the white pumice clasts have higher VNDs than the grey pumices (Table 1). On plots of the volume ratio of vesicles to melt (V_G/V_L after Gardner et al. 1996) versus vesicle number density (Fig. 11), the white and grey pumices cluster as two separate groups. The white pumice is characterised by fairly uniform VND despite slight variations in vesicularity, whereas the grey pumice displays a wider range in VND and more uniform vesicularity. There are no temporal trends in the VND, either between or among pumice types. The variation within any one sample is larger than the differences over time or between pumice types.

In addition to the differences in VND and VVD, the white and grey pumice types display contrasting textures (Figs. 6 and 12). The white pumice generally has no fabric, with only small regions where the vesicles are stretched and oriented in a common direction. Its vesicle population is slightly more homogeneous, clustering around an equivalent vesicle diameter of 50–80 μm (Figs. 6e, f and 8) and separated by thinner (2–10 μm) melt films. The grey pumices, in contrast, are less vesicular and have more mature textures, i.e. more complex vesicle shapes and higher abundances of stretched and oriented vesicles, as well as more regions characterised by trains of vesicles (Fig. 6l, o). Vesicles in grey pumice are separated by thicker (5–15 μm) melt films than in the white pumice, and clusters of vesicles in the grey pumice are separated by 20–40 μm thick glass (Fig. 12). These contrasting textures are also accompanied by differences in crystal content. The grey pumice contains greater abundance of macrocrysts and microlites than the white pumice (Fig. 13b, c).

The grey pumices display further complexity, containing regions characterised by textures of contrasting maturity on length scales of millimetres (Fig. 13). The dominant texture, by area, is more mature, having irregularly shaped vesicles and significantly higher microlite content. The subordinate texture is less mature, with dominantly round and larger vesicles, and fewer microlites, similar to the textures in the white pumice

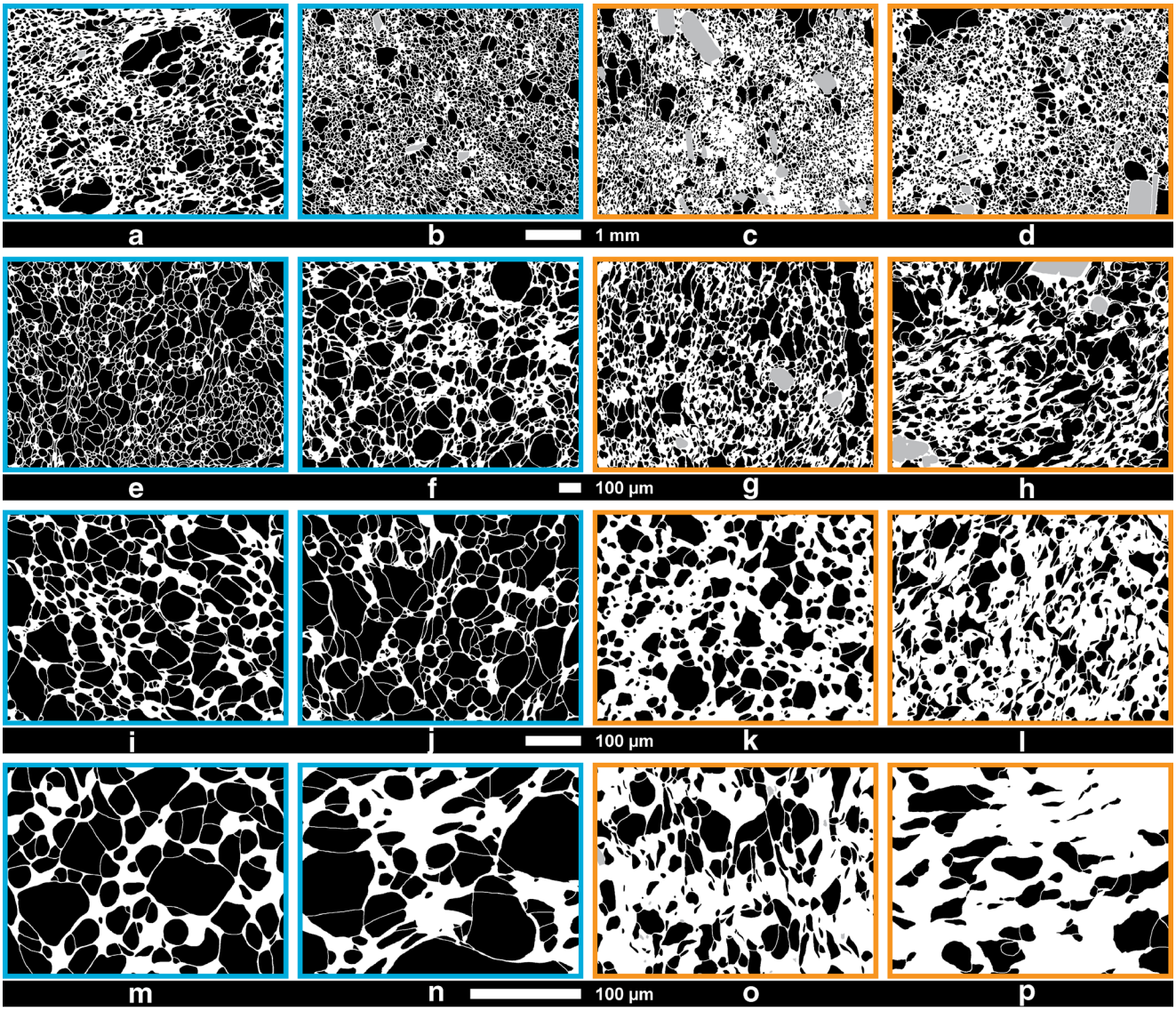

Fig. 6 Range of textures observed in pumice from the Hekla 1158 eruption. Decoalesced images at four different magnifications (a–d 25×, e–h 100×, i–l 250×, and m–p 500×). Vesicles are shown in *black*, glass in *white* and phenocrysts and microphenocrysts in *grey*. Images with *blue outline* are from white pumice, and images with *orange outline* are from grey pumice

(Fig. 13b). The more mature domain has a higher VND, smaller vesicle median diameter, and image vesicularities <50 %, whereas the less mature domain has a lower VND, larger vesicle median diameter, and image vesicularities >50 %. The two domains are intermingled in every clast; the contacts and distinction between the two are most distinct in the two stratigraphically highest samples.

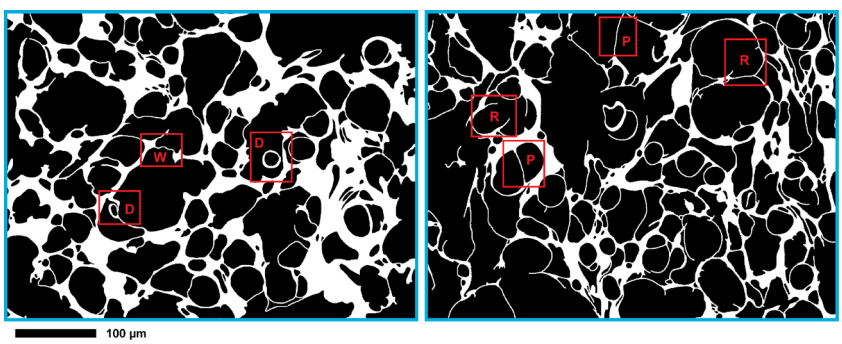

Fig. 7 Coalescence features observed in the Hekla 1158 white pumice: wall rupture (*R*), donuts (*D*), wrinkling (*W*), and planar walls (*P*)

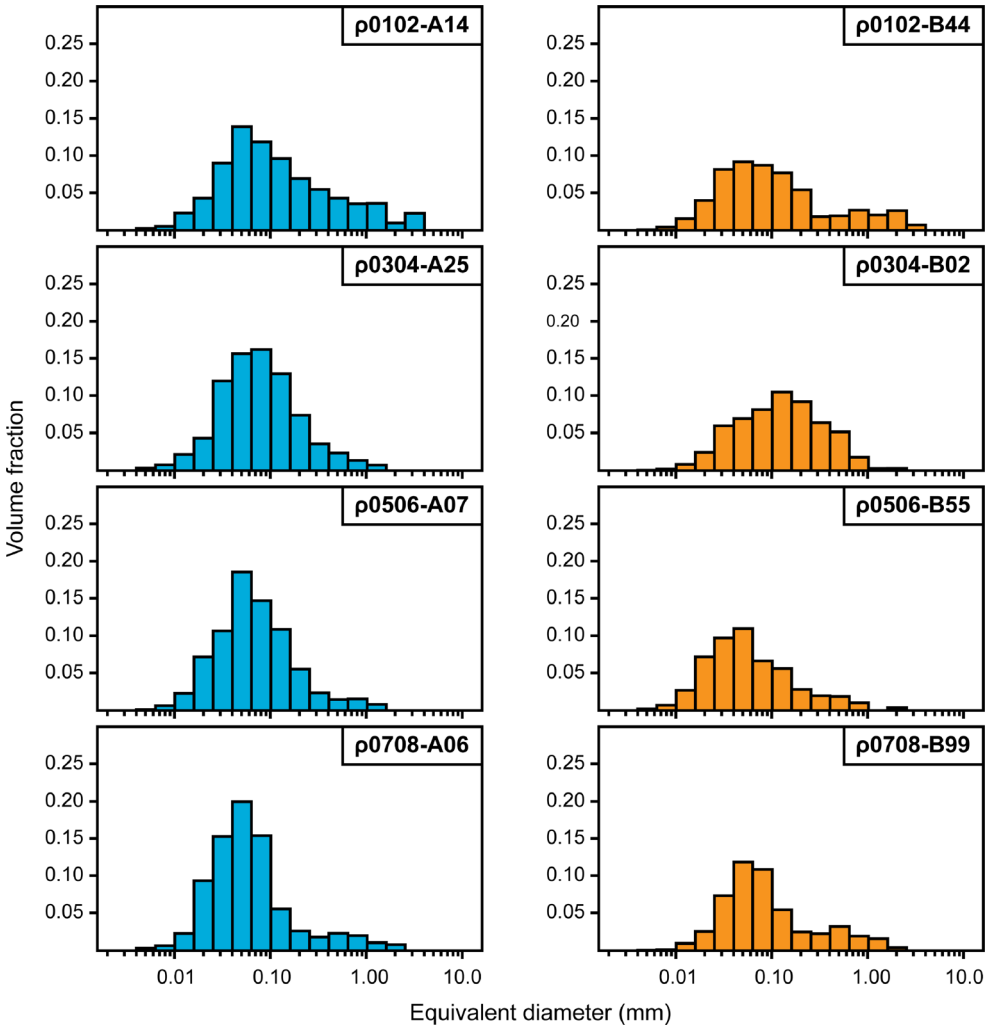

Fig. 8 Vesicle volume distribution for white (*left column*) and grey (*right column*) pumice clasts from the Hekla 1158 eruption. Geometric bins for the equivalent diameters were constructed using a scale factor of $10^{0.1}$

Interpretations and discussion

Implications of grain size, sorting, and componentry

Small upward fining of grain size (decrease in Md_ϕ) and uniform sorting with stratigraphic height (i.e. over time) indicate that the AD 1158 eruption was dry (magmatic) and relatively steady and sustained. After initial rapid onset, the intensity was steady and then declined slightly over the course of the eruption. The observed trend in relative abundance of lithic clasts, together with the grain size data, is interpreted to represent three eruptive stages, namely, initial wall-rock-rich conduit opening and clearing (sample 08), followed by a more stable, steady part of the eruption (samples 07–04) and ending with late-stage vent-wall destabilisation and collapse of the conduit (samples 03–01) as the eruption intensity decreased. The grain size data, as well as the low overall abundance of the wall-rock lithic component (Fig. 3), thus indicate fairly simple eruptive dynamics, similar to that of many subplinian and Plinian eruptions worldwide.

Interpretation of vesicle number and size distribution

A more complex picture of pre- and syn-eruptive dynamics than the one presented above is apparent from the vesicularity data and we explore this in more depth below.

Bubble nucleation

Vesicles start to nucleate at a critical level of volatile supersaturation. Numerical studies and experiments on silicic melts have shown that the VND scales with the degree of volatile supersaturation and thus increases with increasing rate of decompression, i.e. ascent rate (Toramaru 1995, 2006; Mourtada-Bonnefoi and Laporte 1999, 2004; Mangan and Sisson 2000; Mangan et al. 2004b; Hamada et al. 2010). At high supersaturation, nucleation is homogeneous and continuous (Mourtada-Bonnefoi and Laporte 1999, 2002; Mangan and Sisson 2000; Mangan et al. 2004b), resulting in exponential size distributions, where the dominant small vesicle

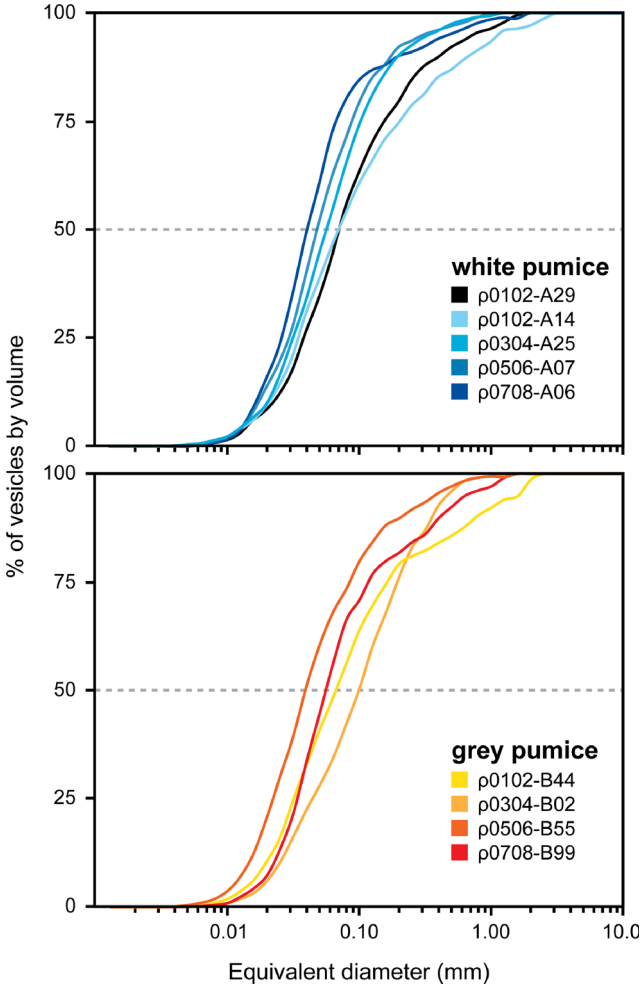

Fig. 9 Cumulative vesicle volume percent plot for white (*top*) and grey pumice (*bottom*). Each *line* represents an individual clast. For each pumice type, colour scheme from *dark* to *light* corresponds to stratigraphic position of sample from lowest to highest, respectively. For the white pumice, the *black line* is the maximum vesicularity clast

subpopulation represents those vesicles that nucleated last. To a first approximation, the VND thus reflects nucleation conditions and the ascent rate immediately prior to fragmentation.

The white pumice clasts have a very narrow range of VND that suggests a common history of late-stage bubble nucleation under very similar conditions for the sampled portion of the melt. Unimodal volume fraction histograms, dominated by small bubbles (Fig. 8), and smooth sigmoidal cumulative vesicle volume curves (Fig. 9) in the white pumice indicate that most of the vesicle nucleation occurred in a single, relatively short stage close to fragmentation, probably during rapid, non-linear acceleration of magma up the conduit. The high VNDs (10^8 to 10^9 cm^{-3}) are comparable to those of more powerful and sustained Plinian phases, e.g. the 1912 Novarupta eruption (Adams et al. 2006) for which Gonnermann and Houghton (2012) inferred that the smallest vesicle population formed within a few 10^{-1} s prior to fragmentation, at decompression rates of 10^7 Pa s^{-1}.

In comparison, the grey pumice shows a significantly wider range of VND values, suggesting either that nucleation rates varied more widely or that the signature of nucleation was variably overprinted by other processes. We present evidence in the "Bubble collapse" section that supports the latter interpretation. The grey pumice clasts have broader unimodal (or weakly bimodal) VVDs (Fig. 8), in which the primary mode is less pronounced and shifted towards slightly larger vesicle sizes. The small (<25 μm) vesicle population, however, amounts to 10 to 30 % of the vesicle volume, indicative that nucleation was still occurring within the melt at the time of fragmentation.

Bubble growth and coalescence

During magma ascent, vesicles increase in size by free growth and by coalescence (Gonnermann and Manga 2007 and references therein). Vesicle growth skews the population towards larger vesicles, and coalescence reduces VND.

The VSD trends (Fig. 10), with larger vesicles following a power law relationship and smaller (<25 μm) vesicles following an exponential trend on log–log plots, are similar to those observed in pumice from the AD 1912 Novarupta eruption (Adams et al. 2006). In general, a single pulse of sustained nucleation and growth results in simple exponential trends (Sarda and Graham 1990; Mangan et al. 1993), whereas power law relationships can be produced by a range of processes, including coalescence and protracted or multiple stages of nucleation (e.g. Cashman and Mangan 1994; Gaonac'h et al. 1996; Simakin et al. 1999; Blower et al. 2001, 2002; Mangan et al. 2004a). The combination of exponential and power law trends in all white pumice clasts suggests that a subpopulation of the earliest nucleated vesicles had sufficient time to interact and undergo limited coalescence, while new, small vesicles were still nucleating. The complex shapes observed in the larger vesicle population, however, indicate that coalescence occurred on time scales shorter than the characteristic viscous relaxation time scale (Larsen and Gardner 2000), preventing vesicles from returning to their spherical state prior to fragmentation.

The grey pumice clasts display VSD trends similar to those of the white pumice (Fig. 10); for two of the clasts, however, the exponential trend ends at larger vesicles (30 and 40 μm) than in the white pumice. The shift of the VVD (Fig. 8) towards a weaker mode at slightly larger vesicle-sizes indicates that the grey melt experienced more prolonged time for vesicle growth and coalescence to occur.

VND is not affected by free growth, but coalescence reduces the VND by creating a few larger vesicles at the expense

Table 1 Vesicularity data for the Hekla 1158 eruption

Clast	Type	Density (kg m^{-3})	Ves.[a] (vol.%)	N_A[b] (cm^{-2})	N_V[c] (cm^{-3})	N_{Vm}[d] (cm^{-3})	Size range[e] (mm)	Median (mm)	No. vesicles included
ρ0102-A29	White	360	84.6	1.70E+5	1.55E+8	1.00E+9	0.004–1.956	0.0719	2765
ρ0102-A14	White	500	78.6	1.80E+5	1.82E+8	8.51E+8	0.004–2.601	0.0713	2422
ρ0102-B44	Grey	1000	57.6	1.47E+5	1.33E+8	3.13E+8	0.004–2.255	0.0663	4312
ρ0304-A25	White	480	79.7	1.87E+5	2.10E+8	1.04E+9	0.004–1.023	0.0576	3026
ρ0304-B02	Grey	980	58.2	8.76E+4	6.72E+7	1.61E+8	0.004–1.347	0.0988	3099
ρ0506-A07	White	550	76.8	2.29E+5	2.02E+8	8.72E+8	0.004–1.021	0.0488	2693
ρ0506-B55	Grey	1130	52.1	2.22E+5	2.26E+8	4.73E+8	0.004–1.260	0.0389	6486
ρ0708-A06	White	500	78.8	2.37E+5	1.96E+8	9.25E+8	0.004–1.890	0.0409	2077
ρ0708-B99	Grey	1150	51.1	1.04E+5	7.36E+7	1.51E+8	0.004–1.316	0.0559	3384

[a] Vesicularity calculated from density and DRE of 2350 kg m^{-3}

[b] Number of vesicles per unit area

[c] Number of vesicles per unit volume of clast matrix, phenocrysts subtracted

[d] Number of vesicles per unit volume, referenced to melt only

[e] Equivalent diameter, assuming a circular cross section area

of smaller vesicles. The trends in Fig. 11 suggest that variability within the dominant subpopulation of small bubbles in the white pumice reflects differing degrees of free growth of originally very similar bubble populations. The grey pumice clasts, however, have more complex vesiculation histories. The range in vesicularity of the white pumice is not accompanied by a significant range in VND, and the diversity within samples is larger than the diversity between samples. The very similar numbers of small bubbles suggest that latest-stage ascent of the magma resulting in the white pumice, immediately prior to fragmentation, occurred under very uniform conditions. The single analysed more vesicular clast has a markedly higher vesicularity (diamond in Fig. 11), reflecting an extended role for free growth of bubbles, but a similar VND to the modal samples, consistent with a relatively simple vesiculation history for all the melt that formed the white pumice. This is in stark contrast to the more complex vesiculation history of the grey pumice (see below).

Bubble collapse

As vesicles continue to increase in size and interact, outgassing can occur via formation of permeable vesicle networks (Eichelberger et al. 1986; Mueller et al. 2005) or by elongate pathways formed by cracking and brittle deformation of the magma (Gonnermann and Manga 2003; Rust et al. 2004). The textures observed in the grey pumice (Figs. 6o, p and 13) support the interpretation that the magma experienced partial outgassing and vesicle collapse. Evidence of vesicle collapse includes thickened interstitial melt between vesicles and pinched appearance of vesicles, features similar to those observed in pumice from the AD 1912 Novarupta (Adams et al. 2006) and the AD 181 Taupo (Houghton et al. 2010) eruptions. Similar textures with thickened interstitial melt and lack of small vesicles, resulting from collapse of micropore networks during outgassing, have also been observed in experiments (Kennedy et al. 2016).

Derived vesicle data supports the conclusion that the grey pumice formed from magma that experienced partial outgassing and vesicle collapse. The volume ratio of vesicles to melt (V_G/V_L) is largely independent of VND, because the small vesicles that drive the VND make a negligible contribution to the total gas volume. Volatile loss through outgassing, however, can collapse large vesicles and thereby decreases V_G/V_L, whereas free growth increases V_G/V_L. The lower V_G/V_L of the grey pumice compared to the white pumice is interpreted to result from onset of vesicle collapse and partial outgassing that is not observed in the white pumice.

Temporal changes during the eruption

The white pumice clasts display several trends with time (i.e. from the stratigraphically lowest to highest sample). VND increases slightly through the first three samples then decreases up section. One interpretation of this change is that the ascent rate, and hence nucleation rate, of the sampled portion of the melt increased slightly over time, followed by a minor decrease towards the end of the eruption. The VVD broadens with time (left side of Fig. 8), and there are corresponding shifts of the CVVD curve (Fig. 9) towards less steep slopes, as well as an increase in the median diameter from 40 to

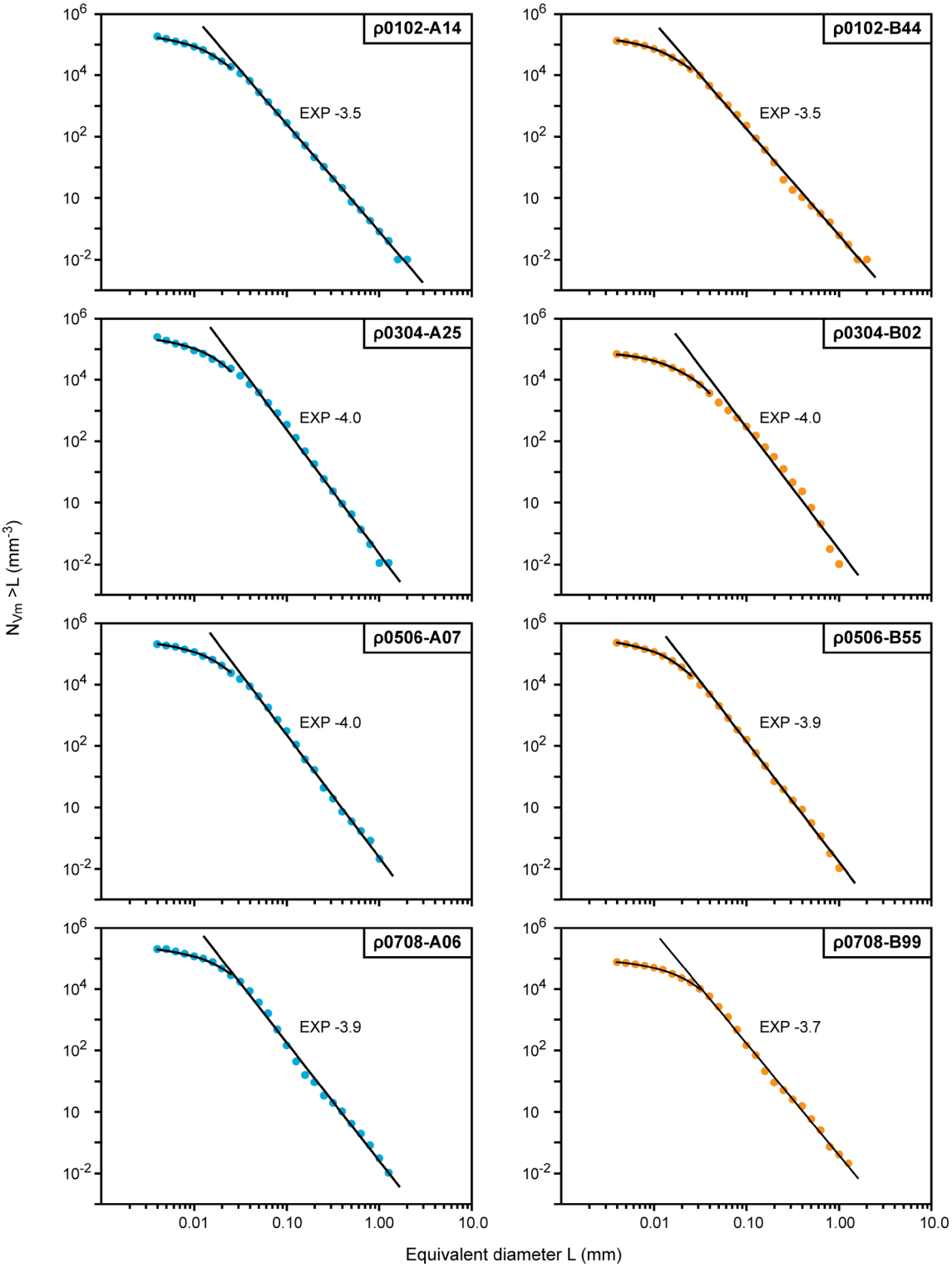

Fig. 10 Cumulative vesicle-size distributions for white (*left*) and grey (*right*) pumice, shown as number of vesicles greater than a given size versus equivalent diameter on a log–log plot. Larger vesicles follow a power law trend, whereas smaller vesicles (<25 and <40 μm for white and grey pumice, respectively) follow an exponential trend. *EXP* exponent of power law trend

70 μm with time. We interpret these relatively smooth and progressive changes, both in the VND and in the CVVD, to reflect increasing time for growth and coalescence during the course of the eruption, associated with a decrease in ascent rate. The textural changes are consistent with the notion that the magma for the white

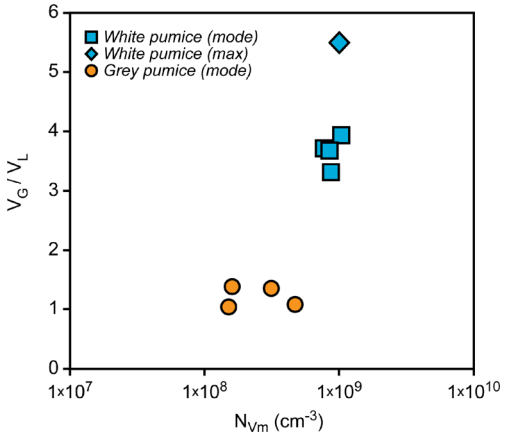

Fig. 11 Volume ratio of vesicles to melt (V_G/V_L) against vesicle number density referenced to melt (N_{vm}) for selected clasts from the Hekla 1158 eruption. White pumice clasts are shown as *blue squares*, grey pumice as *orange circles*. The *blue diamond* is representative of the higher end vesicularity among the white pumice

Fig. 13 **a** Rectified images of contrasting textural domains within grey pumice clasts at two different magnifications. The less mature domain is shown in the *middle column* and the more mature domain in the *right column*. Vesicles are shown in *black*, phenocrysts in *grey* and melt in *white*. Microlites are included as melt. For comparison, *left column* shows images from a white pumice clast at the same stratigraphic level. **b** Non-rectified BSE images of domains within one grey pumice clast, showing contrasting microlite content (examples highlighted with *red arrows*) between less mature domain on the *left* and more mature domain on the *right*. Both images are at the same scale. **c** Non-rectified BSE images of white pumice clast, at two magnifications, showing the difference in microlite content compared to grey pumice

pumice formed a coherent batch that gradually and subtly evolved with time during the eruption.

In contrast, the grey pumice shows no clear temporal trends. Rather than the systematic shift in the CVVD curves observed for the white pumice, the entire curve shifts seemingly randomly back and forth between samples (Fig. 9). The VND also varies more widely from lower and higher values (1.5 to 1.6 × 10^8 versus 3.1 to

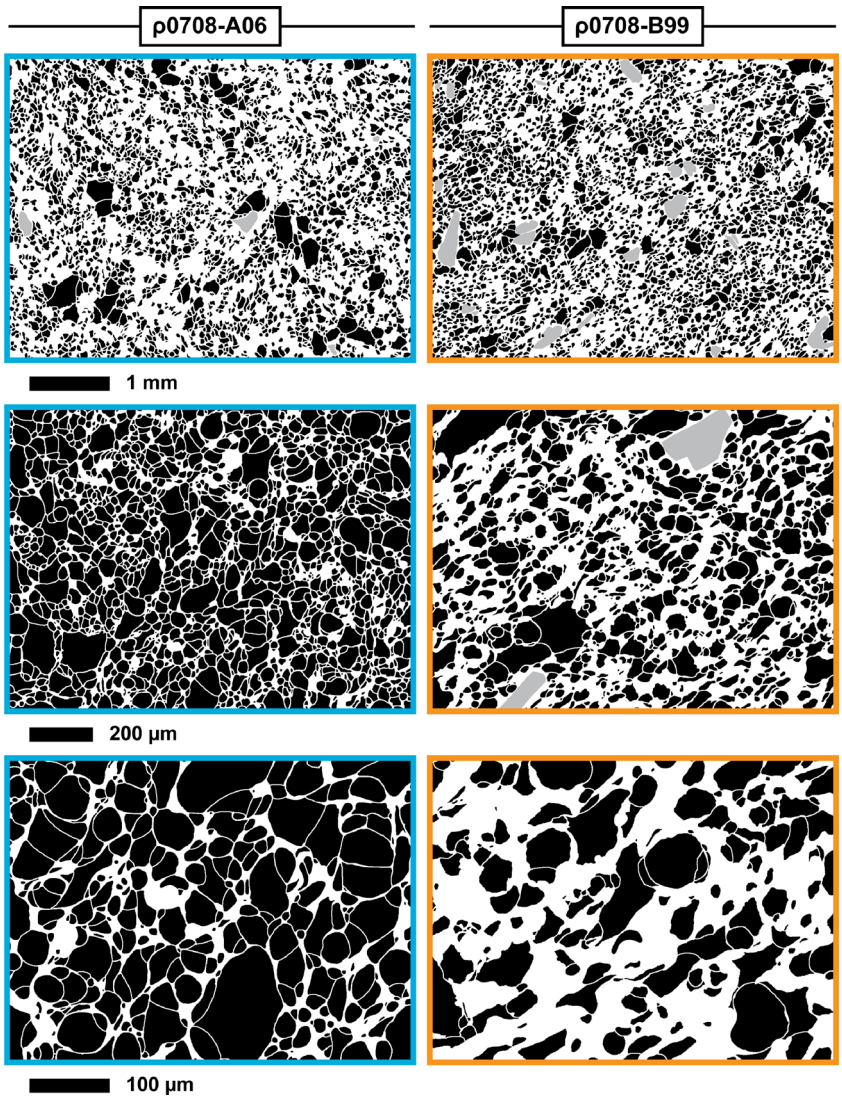

Fig. 12 Comparison of rectified images at three magnifications from a pair of white (*left column*) and grey (*right column*) pumice clasts from the Hekla 1158 eruption. The clasts are from sample ρ0708 (lowermost sample range in Fig. 4a). Vesicles are shown in *black*, phenocrysts in *grey,* and melt in *white*. Microlites are shown as melt. In the lowest magnification images (*top row*), the smallest vesicles below the inclusion limit are depicted as melt

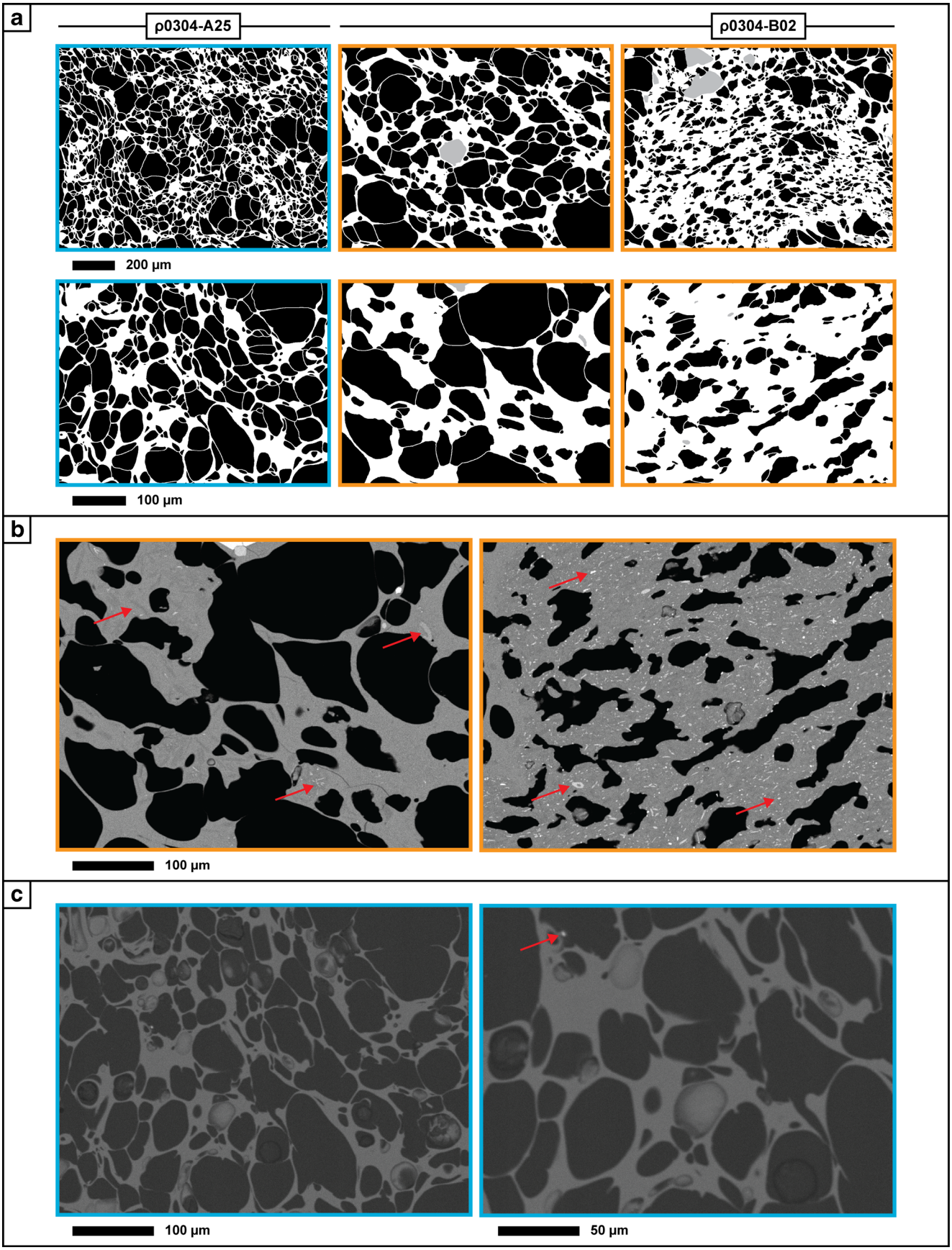
a
ρ0304-A25
ρ0304-B02
200 μm
100 μm
b
100 μm
c
100 μm
50 μm

4.7×10^8 cm^{-3}; Fig. 11; Table 1). Care should be taken not to infer too much regarding any temporal trends, or lack of trends, from the grey pumice clasts because of the relatively low number of clasts that were analysed. However, we think it is likely that the magma from which the grey pumice formed was unsystematically or accidentally incorporated, by the co-eruptive magma resulting in the white pumice, on short time scales during ascent.

Pumice diversity and conduit heterogeneity

Textural differences between the two pumice types, and their vesicle-size distributions and number densities stipulate that the more mature grey pumice textures could have evolved from a magma resembling that of the texturally less mature white pumice but not the other way around.

The two populations do not merge to form a smooth trend on any vesicularity plot (e.g. Fig. 11). Instead, the textural separation between the white and grey pumice in terms of V_G/V_L versus VND (Fig. 11), and their existence as banded clasts, suggests that the two experienced contrasting histories in the shallow plumbing below Hekla and came together at a comparatively late stage in order to mingle and then fragment. The principal distinction between the two populations is a marked difference in the V_G/V_L values (Fig. 11). The grey pumice clasts have markedly lower V_G/V_L values and slightly decreased VND, consistent with a phase of bubble collapse and partial outgassing not experienced by the magma which formed the white pumice.

The limited textural diversity of the white pumice can be explained by varying amounts of free growth of bubble populations formed under very consistent conditions of bubble nucleation throughout the eruption. The diversity in the grey pumice, on the other hand, can be explained by varying degrees of renewed bubble coalescence after a significant amount of bubbles had already been lost by outgassing. The two pumice types thus represent melts with different histories. The grey melt experienced an extended opportunity for crystallisation and bubble coalescence, accompanied by variable amounts of open-system degassing, manifested as a decrease in VND and broadening of the VSD.

Of the grey clasts for which quantitative textural analysis was performed, sample ρ0304-B02 has the highest vesicularity (58 vol.%; Table 1). In addition, it has the largest median vesicle diameter (100 μm) of all analysed clasts, including the more vesicular white pumice clasts. The more mature domain has generally thicker (5–40 μm) interstitial melt than do the other grey clasts, but the less mature domain is significantly more vesicular than the other clasts. The median vesicle diameter of the more mature domain is comparable to that of the other clasts (~40 μm), whereas the median vesicle diameter of the less mature domain is distinctly larger than in the other clasts (90 versus 40–60 μm). We interpret the range in vesicle textures observed in the grey pumice as resulting from a complex protracted intermingling process in which melts of contrasting vesicularity and maturity interact in the conduit. These melts continue to mature up until fragmentation, preserving their original integrity.

Eruption model

The textural diversity observed in the pumice population of the Hekla AD 1158 eruption cannot be explained by a

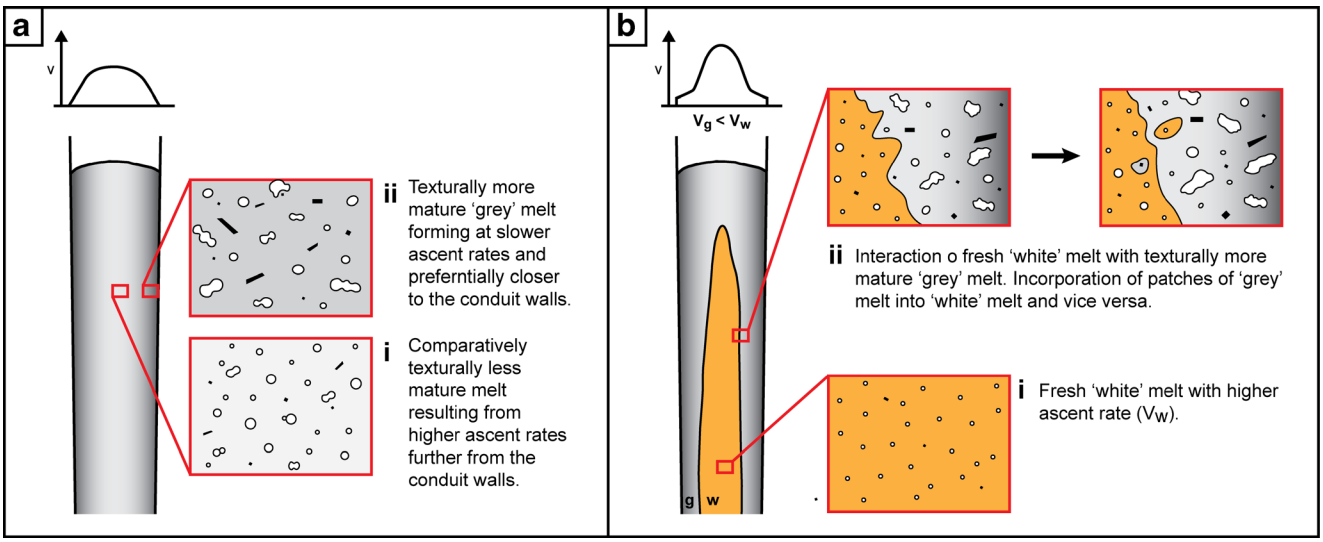

Fig. 14 Cartoon of proposed model for the 1158 Hekla eruption with two stages of ascent prior to fragmentation. **a** Mature texture ('grey melt', close-up *ii*) developing progressively axisymmetrically along the conduit margins through bubble coalescence and degassing of melt ('white', close-up *i*) that stalled or slowed down during ascent. **b** Injection of fresh 'white melt' (*i*) which ascends faster than the more mature melt. Entrainment of pockets of fresh melt into mature melt (*ii*) leading to the domains of contrasting maturity within the grey pumice

traditional Plinian eruption model in which relatively uniform melt rapidly ascends and vesiculates evenly in the shallow conduit. It requires simultaneous fragmentation of melt of contrasting textural maturity and thus residence time in the shallow conduit. We propose that the endmember pumice types correspond to two texturally distinct portions of the melt with different ascent histories that mingled and fragmented together during the eruption. The banded pumice captures the mingling of the two melts during ascent, displaying either sharp interface between white and grey bands or stretched pockets of grey melt in the white melt.

The relatively uniform white pumice is always dominant within the stratigraphy. It represents the newest and more rapidly ascending melt that interacted with melt that had slowed during ascent and experienced increased crystallisation as well as vesicle coalescence and outgassing (Fig. 14). The grey pumice formed by not only slower but also more variable ascent rates. We propose that small packages of more mature melt, along the conduit margins, were overtaken and entrained (close-up ii, Fig. 14b) by the ascending fresh melt over a wide-depth range, thus accounting for the textural diversity and range in VND of the resulting grey pumice. The entrainment process was likely not continuous but occurred repeatedly. As a consequence, some of the rising new melt, together with entrained older melt, slowed sufficiently for coalescence and outgassing to begin, thus evolving into texturally more mature melt at the expense of fresh melt. This incremental process can account for the textural diversity of the grey pumice. In this model, the textural domains of contrasting maturity within many grey pumice clasts resulted from the early mixing of melts of contrasting maturity (Fig. 14b). As the eruption continued, the difference lessened between contrasting grey domains, gradually homogenising the melt filling the conduit.

The relative abundance of white pumice scales inversely with lithic content. The lowest proportion of grey pumice correlates with the inferred peak intensity of the eruption based on grain size (see Fig. 3b–d). We interpret this to reflect a dominant role of the fresh melt during conditions of highest ascent and discharge rate in the middle stages of the eruption. Slower ascent accompanying conduit opening permitted slightly longer residence times during which the melt texture evolved, resulting in the grey pumice. Similar conditions prevailed towards the end of the eruption, when discharge and ascent rates waned.

Conclusions

Based on superficial deposit characteristics, the AD 1158 subplinian eruption of Hekla appears similar to the preceding Plinian eruptions and subplinian opening phases of succeeding eruptions. The variability in the juvenile material, however, indicates a more complex story perhaps linked to the relatively low mass discharge and hence ascent rates. Despite its sustained and relatively steady but short duration, the AD 1158 eruption shows evidence of complex vesiculation and partial outgassing of magma in the shallow conduit. A dominant, newly arrived and erupted ('white') melt was physically homogeneous and characterised by a narrow range of VNDs. A smaller portion of the melt ('grey') developed more evolved textures along the conduit margin. This melt was then entrained by, and mingled with, the dominant fresh melt.

Similar bimodal assemblages of compositionally identical white and grey pumices are common in subplinian–Plinian deposits elsewhere. White pumice is always dominant, microlite free and characterised by larger populations of bubbles that preserve evidence for late-stage coalescence. Grey pumice clasts have thicker bubble walls, round bubble shapes and generally abundant microlites. Such grey pumice is inferred to be derived by heterogeneous flow and degassing but under diverse conditions that include (i) slowed or stalled ascent, either on conduit margins or across the conduit (Hammer et al. 1999; Adams et al. 2006) and (ii) rapid ascent of lower viscosity melt along conduit margins due to marginal viscous heating (Polacci et al. 2001). During (i), protracted degassing, bubble collapse and gas separation can occur during repose intervals of days (Hammer et al. 1999), whereas dynamic processes of bubble shearing, onset of connected permeability, foam collapse and even melt fracturing during (ii) occur on time scales as short as hours (Polacci et al. 2001).

The magma resulting in the grey pumice is, except in the case of the Pinatubo climactic deposit (Hammer et al. 1999), inferred to develop under conditions of extended residence time in the shallow conduit. This permits the development of local domains, first of extended connectivity and then of bubble collapse and outgassing. This is plausibly postulated to occur under conditions that range from relatively static conditions during significant periods of repose (28–262 min before the climactic phase at Pinatubo; Hammer et al. 1999) to ongoing dynamic degassing and outgassing during sustained, although sometimes unsteady eruption. Not surprisingly, relatively static conditions appear more common with low mass eruption rate, such as during many subplinian eruptions. In the case of the Hekla AD 1158 eruption, where a sustained discharge rate is clearly indicated, we favour the latter scenario. This type of eruption therefore lie in the middle ground between more powerful Plinian events characterised by relatively few and very closely spaced eruptive phases, e.g. the first two Plinian phases of the Novarupta AD 1912 eruption (Adams et al. 2006) and the Taupo AD 181 eruption (Houghton et al. 2010) and weaker eruptions in which the explosive interval is divided into relatively short pulses separated by repose intervals of less than 1 day (Hammer et al. 1999). During the more powerful phases, the extent of bubble

nucleation, growth, and coalescence remains relatively uniform in time and space. More texturally mature melt is therefore not developed, resulting in a uniform population of white pumice clasts. In contrast, during the weaker eruptions, the wider range of ascent and storage conditions creates a more diverse clast assemblage that still contains white pumice but also contains a population of grey pumice.

Acknowledgments This research was funded by the National Science Foundation grant EAR12-20596. The manuscript was significantly enhanced by insightful reviews by editor J. Gardner and two anonymous reviewers, and comments from D. A. Swanson and S. A. Fagents. The authors are grateful to Carolyn Parcheta for assistance with fieldwork; Isaac Ishihara for density analysis; JoAnn Sinton for thin section polishing; and Eva Kakone, Hannah Azouz, and Jaclyn Guenther for image processing.

References

Adams NK, Houghton BF, Hildreth W (2006) Abrupt transitions during sustained explosive eruptions: examples from the 1912 eruption of Novarupta, Alaska. B Volcanol 69:189–206

Blower JD, Keating JP, Mader HM, Phillips JC (2001) Inferring volcanic degassing processes from vesicle size distributions. Geophys Res Lett 28:347–350

Blower JD, Keating JP, Mader HM, Phillips JC (2002) The evolution of bubble size distributions in volcanic eruptions. J Volcanol Geoth Res 120:1–23

Cashman KV, Mangan MT (1994) Physical aspects of magmatic degassing; II, constraints on vesiculation processes from textural studies of eruptive products. Rev Mineral Geochem 30:447–478

Eichelberger JC, Carrigan CR, Westrich HR, Price RH (1986) Non-explosive silicic volcanism. Nature 323:598–602

Gaonac'h H, Lovejoy S, Stix J, Scherzter D (1996) A scaling growth model for bubbles in basaltic lava flows. Earth Planet Sc Lett 139: 395–409

Gardner JE, Thomas RM, Jaupart C, Tait S (1996) Fragmentation of magma during Plinian volcanic eruptions. B Volcanol 58:144–162

Gonnermann HM, Houghton BF (2012) Magma degassing during the Plinian eruption of Novarupta, Alaska, 1912. Geochem Geophy Geosy. doi:10.1029/2012GC004273

Gonnermann HM, Manga M (2003) Explosive volcanism may not be an inevitable consequence of magma fragmentation. Nature 426:432–435

Gonnermann HM, Manga M (2007) The fluid mechanics inside a volcano. Annu Rev Fluid Mech 39:321–356

Gronvold K, Larsen G, Einarsson P, Thorarinsson S, Saemundsson K (1983) The Hekla eruption 1980–1981. B Volcanol 46:349–363

Gudmundsdóttir ER, Larsen G, Eiríksson J (2011) Two new Icelandic tephra markers: the Hekla Ö tephra layer, 6060 cal. yr BP, and Hekla DH tephra layer, ~6650 cal. yr BP. Land–sea correlation of mid-Holocene tephra markers. The Holocene 21:629–639

Hamada M, Laporte D, Cluzel N, Koga KT, Kawamoto T (2010) Simulating bubble number density of rhyolitic pumices from Plinian eruptions: constraints from fast decompression experiments. B Volcanol 72:735–746

Hammer JE, Cashman KV, Hoblitt RP, Newman S (1999) Degassing and microlite crystallization during pre-climactic events of the 1991 eruption of Mt. Pinatubo, Philippines. B Volcanol 60:355–380

Höskuldsson Á, Óskarsson N, Pedersen R, Grönvold K, Vogfjörð K, Ólafsdóttir R (2007) The millennium eruption of Hekla in February 2000. B Volcanol 70:169–182

Houghton BF, Wilson CJN (1989) A vesicularity index for pyroclastic deposits. B Volcanol 51:451–462

Houghton BF, Carey RJ, Cashman KV, Wilson CJN, Hobden BJ, Hammer JE (2010) Diverse patterns of ascent, degassing, and eruption of rhyolite magma during the 1.8 ka Taupo eruption, New Zealand: evidence from clast vesicularity. J Volcanol Geoth Res 195:31–47

Inman DL (1952) Measures for describing the size distribution of sediments. J Sediment Petrol 22:125–145

Janebo MH, Thordarson T, Houghton BF, Bonadonna C, Larsen G, Carey RJ (2016) Dispersal of key subplinian–Plinian tephras from Hekla volcano, Iceland: implications for eruption source parameters. B Volcanol 78:66. doi:10.1007/s00445-016-1059-7

Kenney BM, Wadsworth FB, Vasseur J, Schipper CI, Jellinek AM, von Aulock FW, Hess K-U, Russell JK, Lavallée Y, Nichols ARL, Dingwell DB (2016) Surface tension driven processes densify and retain permeability in magma and lava. Earth Planet Sc Lett 433: 116–124

Klug C, Cashman KV (1994) Vesiculation of May 18, 1980, Mount St. Helens magma. Geology 22:468–472

Klug C, Cashman KV, Bacon CR (2002) Structure and physical characteristics of pumice from the climactic eruption of Mount Mazama (Crater Lake), Oregon. B Volcanol 64:486–501

Larsen G (1992) Gjóskulagid úr Heklugosinu 1158 (the tephra layer from the 1158 AD eruption of Hekla). Jardfrædafélag Islands, Vorrádstefna, Yfirlit og Ágrip Reykjavik: Geoscience Society of Iceland 25–27

Larsen G (2002) A brief overview of eruptions from ice-covered and ice-capped volcanic systems in Iceland during the past 11 centuries: frequency, periodicity and implications. Geol Soc Lond, Spec Publ 202:81–90

Larsen G, Eiríksson J (2008a) Holocene tephra archives and tephrochronology in Iceland—a brief overview. Jokull 58:229–250

Larsen G, Eiríksson J (2008b) Late Quaternary terrestrial tephrochronology of Iceland—frequency of explosive eruptions, type and volume of tephra deposits. J Quat Sci 23:109–120

Larsen JF, Gardner JE (2000) Experimental constraints on bubble interactions in rhyolite melts: implications for vesicle size distributions. Earth Planet Sc Lett 180:201–214

Larsen G, Thorarinsson S (1977) H4 and other acid Hekla tephra layers. Jokull 27:28–46

Larsen G, Vilmundardóttir EG (1992) Hekla tephra layers from the period 2900–1800 BP: H-x, H-y and H-z. The 20th Nordic Geological Winter Meeting, Abstracts 106, Reykjavík, Iceland.

Larsen G, Dugmore A, Newton A (1999) Geochemistry of historical-age silicic tephras in Iceland. The Holocene 9:463–471

Lirer L, Pescatore T, Booth B, Walker GPL (1973) Two Plinian pumice-fall deposits from Somma-Vesuvius, Italy. Geol Soc Am Bull 84: 759–772

Mangan M, Sisson T (2000) Delayed, disequilibrium degassing in rhyolite magma: decompression experiments and implications for explosive volcanism. Earth Planet Sc Lett 183:441–455

Mangan MT, Cashman KV, Newman S (1993) Vesiculation of basaltic magma during eruption. Geology 21:157–160

Mangan M, Mastin L, Sisson T (2004a) Gas evolution in eruptive conduits: combining insights from high temperature and pressure decompression experiments with steady-state flow modeling. J Volcanol Geoth Res 129:23–36

Mangan MT, Sisson TW, Hankins WB (2004b) Decompression experiments identify kinetic controls on explosive silicic eruptions. Geophys Res Lett. doi:10.1029/2004GL019509

Mourtada-Bonnefoi CC, Laporte D (1999) Experimental study of homogeneous bubble nucleation in rhyolitic magmas. Geophys Res Lett 26:3505–3508

Mourtada-Bonnefoi CC, Laporte D (2002) Homogeneous bubble nucleation in rhyolitic magmas: an experimental study of the effect of H_2O and CO_2. J Geophys Res. doi:10.1029/2001JB000290

Mourtada-Bonnefoi CC, Laporte D (2004) Kinetics of bubble nucleation in a rhyolitic melt: an experimental study of the effect of ascent rate. Earth Planet Sc Lett 218:521–537

Mueller S, Melnik O, Spieler O, Scheu B, Dingwell DB (2005) Permeability and degassing of dome lavas undergoing rapid decompression: an experimental determination. B Volcanol 67:526–538

Polacci M, Papale P, Rosi M (2001) Textural heterogeneities in pumices from the climactic eruption of Mount Pinatubo, 15 June 1991, and implications for magma ascent dynamics. B Volcanol 63:83–97

Róbertsdóttir BG, Larsen G, Eiríksson J (2002) A new detailed stratigraphical and geochemical record of 30 tephra layers from the Hekla volcanic system, Iceland, 2980–850 cal. BP. The 25th Nordic Geological Winter Meeting, Abstracts 178, Reykjavik, Iceland.

Rust AC, Cashman KV, Wallace PJ (2004) Magma degassing buffered by vapor flow through brecciated conduit margins. Geology 32:349–352

Sahagian DL, Proussevitch A (1998) 3D particle size distributions from 2D observations: stereology for natural application. J Volcanol Geoth Res 84:173–196

Sarda P, Graham D (1990) Mid-ocean ridge popping rocks: implications for degassing at ridge crests. Earth Planet Sc Lett 97:268–289

Schneider CA, Rasband WS, Eliceiri KW (2012) NIH image to ImageJ: 25 years of image analysis. Nat Methods 9:671–675

Shea T, Houghton BF, Gurioli L, Cashman KV, Hammer JE, Hobden BJ (2010) Textural studies of vesicles in volcanic rocks: an integrated methodology. J Volcanol Geoth Res 190:271–289

Sigmarsson O, Condomines M, Fourcade S (1992) A detailed Th, Sr and O isotope study of Hekla: differentiation processes in an Icelandic volcano. Contrib Mineral Petr 112:20–34

Simakin AG, Armienti P, Epel'baum MB (1999) Coupled degassing and crystallization: experimental study at continuous pressure drop, with application to volcanic bombs. B Volcanol 61:275–287

Thorarinsson S (1967) The eruptions of Hekla in historical times: a tephrochronological study. In: Einarsson T, Kjartansson G, Thorarinsson S (eds) The eruption of Hekla 1947–1948. Societas Scientiarum Islandica I, Leiftur, Reykjavík, pp. 1–177

Thordarson T, Höskuldsson Á (2008) Postglacial volcanism in Iceland. Jokull 58:197–228

Thordarson T, Larsen G (2007) Volcanism in Iceland in historical time: volcano types, eruption styles and eruptive history. J Geodyn 43: 118–152

Toramaru A (1995) Numerical study of nucleation and growth of bubbles in viscous magmas. J Geophys Res-Sol Ea 100:1913–1931

Toramaru A (2006) BND (bubble number density) decompression rate meter for explosive volcanic eruptions. J Volcanol Geoth Res 154: 303–316

Wright HMN, Folkes CB, Cas RAF, Cashman KV (2011) Heterogeneous pumice populations in the 2.08-Ma Cerro Galán Ignimbrite: implications for magma recharge and ascent preceding a large-volume silicic eruption. B Volcanol 73:1512–1533